Electronic Supplementary Information

Medium Band-Gap Non-fullerene Acceptors Based on Benzothiophene Donor Moiety Enabling High-Performance Indoor Organic Photovoltaics

Xiaojun Li,[a b c] Siwei Luo,[a b g] Huiliang Sun,[d h]* Herman Ho-Yung Sung,[e] Han Yu,[a b g] Tao Liu,[a b g] Yiqun Xiao,[f] Fujin Bai,[a b g] Mingao Pan,[a b g] Xinhui Lu,[f] Ian Duncan Williams,[e] Xugang Guo[d], Yongfang Li,[c] He Yan[a b g]*

[a] Hong Kong University of Science and Technology-Shenzhen Research Institute, No. 9 Yuexing first RD, Hi-tech Park, Nanshan, Shenzhen 518057, P. R. China;

[b] Department of Chemistry, Guangdong-Hong Kong-Macao Joint Laboratory of Optoelectronic and Magnetic Functional Materials, Energy Institute and Hong Kong Branch of Chinese National Engineering Research Center for Tissue Restoration & Reconstruction, Hong Kong University of Science and Technology, Clear Water Bay, Kowloon, Hong Kong;

[c] Beijing National Laboratory for Molecular Sciences, CAS Key Laboratory of Organic Solids, Institute of Chemistry, Chinese Academy of Sciences Beijing 100190, China;

[d] Department of Materials Science and Engineering, Southern University of Science and Technology (SUSTech)No. 1088, Xueyuan Road, Shenzhen, Guangdong 518055, P. R. China;

[e] Department of Chemistry, Hong Kong University of Science and Technology, Clear Water Bay, N. T., Hong Kong SAR, China;

[f] Department of Physics, Chinese University of Hong Kong, New Territories, Hong Kong, China;

[g] Institute of Polymer Optoelectronic Materials and Devices, State Key Laboratory of Luminescent Materials and Devices, South China University of Technology (SCUT), Guangzhou 510640, P. R. China.

[h] Center for Advanced Analytical Science, School of Chemistry and Chemical Engineering, Guangzhou University, Guangzhou 510006, China.

E-mail: Sunhl@sustech.edu.cn (H.S.), hyan@ust.hk (H.Y.)

Methods

Materials and synthesis: All chemicals and solvents were purchased from Innochem, J&K, Alfa Aesar and TCI Chemical Co. respectively. The solvents do not need to degas in all the reactions, and the reactions all performed under a nitrogen atmosphere. Compound 1 was synthesized according to the procedures reported in the literatures. The synthetic route of BT-DF and BT-SCl were shown in Figure 1 and detailed synthesis processes are described in the following.

Synthesis of Compound 2: Compound **1** (2.60g, 10mmol) and 4,7-dibromo-5,6-dinitro[2,1,3]benzothiadiazole (1.52g, 4mmol) were dissolved in toluene (30 mL) under a nitrogen atmosphere. Then an aqueous solution of K_2CO_3 (2M) was added, and the reaction mixture was stirred for 24h at 90℃. Then the mixture was extracted with dichloromethane (100 mL × 3) and water (100 mL), the collected organic layer was dried over $MgSO_4$. After removal of the solvent under reduced pressure, the residue was purified by column chromatography in a silica gel column using petroleum ether/dichloromethane (3:1,v/v) as the eluent to give an orange product **3** (1.6g, 82% yield). ^{1}H NMR (400 MHz, $CDCl_3$) δ 8.14 (s, 2H), 8.01 (d, J = 8.2 Hz, 2H), 7.64 (d, J = 5.5 Hz, 2H), 7.56 (dd, J = 8.3, 1.6 Hz, 2H), 7.46 (d, J = 5.5 Hz, 2H). ^{13}C NMR (101 MHz, $CDCl_3$) δ 153.22, 141.00, 140.17, 129.30, 129.01, 126.15, 124.89, 124.24, 123.80, 123.69. EI m/z calcd for $[M]^+$ $C_{22}H_{10}N_4O_4S_3$ 489.9864 found 489.9832.

Synthesis of Compound 3: Under argon, compound **2** (0.49g, 1mmol) and triphenylphosphine (2.62g, 10mmol) were dissolved in 1,2- dichlorobenzene (o-DCB, 6ml). The mixture was stirred at 180℃ overnight. After cooled to ambient temperature, the solvent was removed under reduced pressure, which gave an orange solid. The orange intermediate was transferred to a three-neck flask, to which potassium carbonate (1.38g, 10mmol), potassium iodide (0.16g, 1mmol), 1-bromo-2-hexyldecane (3.05g, 10mmol) and DMF (6 ml) were added. The mixture was stirred at 90℃ overnight under argon atmosphere. Then the mixture was extracted with dichloromethane (100 ml × 3) and water (100 ml), the collected organic layer was dried over $MgSO_4$. Compound **3** was obtained by column chromatography in a silica gel column using petroleum ether/dichloromethane (10:1,v/v) as the eluent (0.45g, 51% yield). ^{1}H NMR (400 MHz, $CDCl_3$) δ 8.77 (d, J = 8.3 Hz, 2H),

7.94 (d, J = 8.3 Hz, 2H), 7.60 (d, J = 5.3 Hz, 2H), 7.52 (d, J = 5.4 Hz, 2H), 4.88 (s, 4H), 1.88 (s, 2H), 1.20-0.04 (m, 60H). ^{13}C NMR (101 MHz, $CDCl_3$) δ 149.61, 138.73, 136.57, 133.50, 125.37, 124.42, 123.63, 123.48, 123.30, 119.26, 119.16, 118.98, 112.69, 77.40, 77.08, 76.76, 53.87, 38.47, 31.80, 31.58, 31.16, 29.71, 29.37, 29.19, 26.38, 23.94, 22.62, 14.16, 13.95. HRMS (TOF) m/z calcd for $[M]^+$ $C_{54}H_{74}N_4S_3$ 874.5076, found 874.5048.

Synthesis of Compound 4: A Vilsmeier reagent, which was prepared with $POCl_3$ (0.62 mL, 6.4 mmol) in DMF (2.00 mL, 25.84 mmol), was added to a cold solution of Compound **3** (262 mg, 0.3 mmol) in dry 1,2-dichloroethane (20 mL) at 0 °C under a nitrogen atmosphere. After being stirred at 80 °C for 36 h, the mixture was poured into ice water (100 mL), neutralized with Na_2CO_3, and then extracted with dichloromethane. The combined organic layer was washed with water and brine, dried over anhydrous $MgSO_4$. After removal of solvent, it was purified by column chromatography on silica gel using petroleum ether/dichloromethane (1:1) as eluent, yielding a yellow solid **4.** (0.23 g, 83% yield). ^{1}H NMR (400 MHz, $CDCl_3$) δ 10.21 (s, 2H), 8.86 (d, J = 8.4 Hz, 2H), 8.28 (s, 2H), 8.03 (d, J = 8.5 Hz, 2H), 4.93 (s, 4H), 1.85 (s, 2H), 1.13 – -0.04 (m, 60H). ^{13}C NMR (101 MHz, $CDCl_3$) δ 184.06, 149.40, 141.32, 137.68, 136.03, 135.83, 134.19, 128.30, 125.83, 121.17, 120.46, 113.32, 54.18, 38.68, 31.71, 31.47, 30.80, 29.62, 29.32, 29.23, 28.93, 26.12, 23.76, 22.55, 14.10, 13.92. HRMS (TOF) m/z calcd for $[M]^+$ $C_{56}H_{74}N_4O_2S_3$ 930.4974, found 930.4912.

Synthesis of BT-DF: Compound **4** (93 mg, 0.1 mmol) and 2-(5,6-difluoro-3-oxo-2,3-dihydro-1H-inden-1-ylidene) malononitrile (115 mg, 0.5 mmol) were dissolved in $CHCl_3$ (25 mL) under a nitrogen atmosphere. 0.6 ml pyridine was added and refluxed for 2 h. Then, the mixture was poured into water (100 mL) and extracted with $CHCl_3$ (2 × 100 mL). The organic layer was washed with water, and then dried over $MgSO_4$. After removing the solvent, the residue was purified using column chromatography on silica gel employing petroleum ether/$CHCl_3$ (1:4) as an eluent, yielding a dark blue solid **BT-DF** (124 mg, 92%). ^{1}H NMR (400 MHz, $CDCl_3$) δ 9.17 (s, 2H), 8.86 (d, J = 8.5 Hz, 2H), 8.62 (dd, J = 9.8, 6.4 Hz, 2H), 8.41 (s, 2H), 8.01 (d, J = 8.5 Hz, 2H), 7.82 (t, J = 7.4 Hz, 2H), 5.22 (s, 2H), 4.91 (s, 2H), 1.97 (s, 2H), 1.47 – -0.08 (m, 60H). ^{13}C NMR (101 MHz, $CDCl_3$) δ 185.29, 157.38, 155.52, 152.96, 148.75, 143.89, 138.41, 136.83, 136.28, 134.77, 134.55, 134.14,

134.01, 133.21, 126.25, 122.75, 120.44, 120.40, 114.67, 114.46, 113.38, 113.31, 113.20, 112.34, 112.17, 70.79, 53.95, 38.51, 30.98, 29.50, 28.76, 26.47, 23.15, 22.02, 13.44, -0.64. HRMS (TOF) m/z calcd for $[M]^+$ $C_{80}H_{78}F_4N_8O_2S_3$ 1354.5346, found 1354.5349.

Synthesis of BT-SCl: Compound **4** (93 mg, 0.1 mmol) and 2-(5 or 6-chloro-3-oxo-2,3-dihydro-1H-inden-1-ylidene)malononitrile (114 mg, 0.5 mmol) were dissolved in $CHCl_3$ (25 mL) under a nitrogen atmosphere. 0.6 ml pyridine was added and refluxed for 2 h. Then, the mixture was poured into water (100 mL) and extracted with $CHCl_3$ (2 × 100 mL). The organic layer was washed with water, and then dried over $MgSO_4$. After removing the solvent, the residue was purified using column chromatography on silica gel employing petroleum ether/$CHCl_3$ (1:4) as an eluent, yielding a dark blue solid **BT-SCl** (121 mg, 90%).^{1}H NMR (400 MHz, $CDCl_3$) δ 9.19 (d, *J* = 3.5 Hz, 2H), 8.86 (dd, *J* = 8.5, 1.1 Hz, 2H), 8.73 (dd, *J* = 12.3, 5.0 Hz, 2H), 8.41 (s, 2H), 8.00 (dd, *J* = 8.3, 7.0 Hz, 4H), 7.79 (dd, *J* = 8.4, 1.8 Hz, 2H), 5.23 (s, 2H), 4.91 (s, 2H), 1.97 (s, 2H), 1.44 – -0.09 (m, 60H). ^{13}C NMR (101 MHz, $CDCl_3$) δ 186.35, 186.28, 158.42, 158.11, 148.77, 143.64, 141.75, 141.07, 140.78, 138.67, 137.83, 137.60, 136.82, 134.74, 134.56, 134.31, 134.12, 133.12, 126.16, 124.95, 124.38, 123.49, 123.26, 123.21, 120.39, 120.32, 113.66, 113.51, 113.32, 76.70, 76.38, 76.07, 70.98, 70.29, 53.93, 38.50, 30.97, 28.77, 26.41, 23.09, 22.06, 13.48, -0.63. HRMS (TOF) m/z calcd for $[M]^+$ $C_{80}H_{80}Cl_2N_8O_2S_3$ 1350.4943, found 1350.4907.

Measurements: ^{1}H NMR spectra were measured on a Bruker DMX-400 spectrometer with *d*-chloroform as the solvent and trimethylsilane as the internal reference. Mass spectra were recorded on a Shimadzu spectrometer. UV-vis absorption spectra of active layers of the all PSCs were measured on a Hitachi U-3010 UV-vis spectrophotometer. The electrochemical cyclic voltammetry was performed on a Zahner IM6e Electrochemical Workstation, in an acetonitrile solution of 0.1 mol/L *n*-Bu_4NPF_6 at a potential scan rate of 100 mV/s with an Ag/AgCl reference electrode and a platinum wire counter electrode. AFM measurements were obtained by using a Dimension Icon AFM (Bruker) in a tapping mode. The grazing incidence X-ray scattering (GIWAXS) measurement was carried out with a Xeuss 2.0 SAXS/WAXS laboratory beamline using a Cu X-ray source (8.05 keV, 1.54 Å) and a Pilatus3R 300K detector. The incident angle was 0.2°. The samples for GIWAXS measurements were fabricated on silicon substrates using the same recipe for the devices. The

electron and hole mobility were measured by using the method of space-charge limited current (SCLC) for electron-only devices with the structure of ITO/ZnO/active layer/PNDIT-F3N/Ag and hole-only devices with the structure of ITO/PEDOT:PSS/active layer/MoO_3/Ag. The charge carrier mobility was determined by fitting the dark current to the model of a single carrier SCLC according to the equation: $J = 9\varepsilon_0\varepsilon_r\mu V^2/8d^3$, where J is the current density, d is the film thickness of the active layer, μ is the charge carrier mobility, ε_r is the relative dielectric constant of the transport medium, and ε_0 is the permittivity of free space. $V = V_{app} - V_{bi}$, where V_{app} is the applied voltage, V_{bi} is the offset voltage. The carrier mobility can be calculated from the slope of the $J^{1/2} \sim V$ curves.

Experimental of Single Crystal XRD

A suitable single crystal of **LBT-DF**, $C_{80}H_{74}F_4N_8O_2S_3$, was selected and mounted on a SuperNova, Dual, Cu-Kα, Atlas diffractometer. The crystal was kept at 173.0(1) K during data collection. Using Olex2[1], the structure was solved with the olex2.solve[2] structure solution program using Charge Flipping and refined with the SHELXL[3] refinement package using Least Squares minimisation.

The disorder issue of the hydrocarbon chains is explained here. The two branches C_8H_{17} and C_6H_{13}, which originated from C(30), where refined as C(31) to C(38) and C(41) to C(48) with partial occupancies at specific carbon as below:

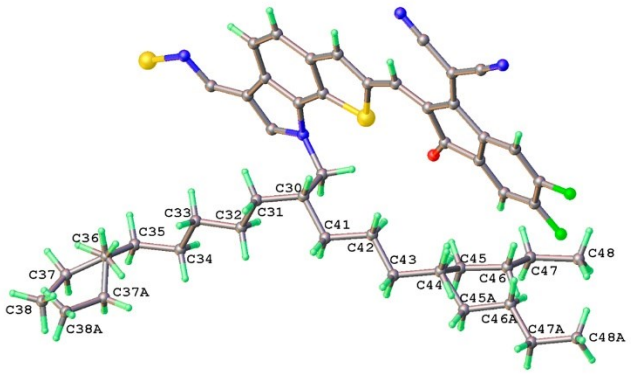

With the branch of C(31) to C(38), C(31) to C(36) are fully occupied, and the split tail refined as a half occupancy of C(37) [0.27] plus C(37A) [0.23] and again a half occupancy of C(38) [0.27] and C(38A) [0.23]. For the another branch of C(41) to C(48), C(41) to C(44) are fully occupied, and

the split tail refined as a full carbon of C(45) [0.65] plus C(45A) [0.35], and again a full carbon of C(46) [0.65] plus C(46A) [0.35], followed by a half occupancy of C(47) [0.25] plus C(47A) [0.25] and again a half occupancy of C(48) [0.25] and C(48A) (0.25). That means the first six carbons of both branches are full carbons and the last two carbons are half carbons, which could be highly probable for the situation of the disordered of C_8H_{17} and C_6H_{13} between the two branches statistically.

Device fabrication and characterization: The PSCs were fabricated with a structure of ITO/PEDOT: PSS (40 nm)/active layer/ PNDIT-F3N/cathode. The ITO was purchased from Shaanxi Fangdecheng Construction Engineering Company. The sheet resistance is 15 Ω and the transmission is around 93%. A thin layer of PEDOT: PSS was deposited through spin-coating on precleaned ITO-coated glass from a PEDOT: PSS aqueous solution (Baytron P VP AI 4083 from H. C. Starck) at 4000 rpm and dried subsequently at 150 °C for 15 min in air. Then the device was transferred to a nitrogen glove box, where the active blend layer of S2 polymer and acceptors was spin-coated from its chloroform solution onto the PEDOT: PSS layer under a spin-coating rate of 3000 rpm. After spin-coating, the active layers were annealed at 100 ^{o}C for 5 min for the devices with thermal annealing treatment. Then methanol solution of PNDIT-F3N at a concentration of 1.0 mg mL^{-1} was deposited atop the active layer at 3000 rpm for 30 s to afford a PDINO cathode buffer layer with thickness of *ca*. 10 nm. Finally, top Al electrode was deposited in vacuum onto the cathode buffer layer at a pressure of *ca*. 5.0×10^{-5} Pa. The active area of the device was 5.9 mm².

Device Testing: For the 1-sun device performance, *J-V* characteristics weremeasured under AM1.5G (100 $mWcm^{-2}$) using a Newport Class A solar simulator (94021A, a Xenon lamp with an AM1.5G filter) in air at room temperature. A standard Si diode with KG5 filter was purchased from PV Measurements and calibrated by Newport Corporation. The light intensity was calibrated using the Si diode as a reference cell to bring the spectralmismatch to unity. *J-V* characteristics were recorded using a Keithley 2400 source meter unit. EQEs were measured using an Enlitech QE-S EQE system equipped with a standard Si diode. Monochromatic light was generated from a Newport 300 W lamp source. These test protocols are the same as those previously used for certified OPVs.

For the indoor performance, *J-V* characteristic curves were measured under an intensity adjustable 2600K LED in dark room at room temperature. The emission power spectrum of this LED at different light intensity was measured by a fiber optics spectrometer. All the cells are measured with a 5.9 mm^2 shadow mask. The emission power spectra, illumination intensities and photon flux spectrum of LED were measured by using calibrated Ocean optics Spectrometer. With these data and IPCE spectrum, the integral current density can be calculated, the details of the calculations are provided as fllows:

Calculation process of the calculated J_{sc}

The integrated current density (J_{cal}) was obtained based on following equations:

$$J_{sc}\,(calculated) = \int EQE(\lambda) * \Phi(\lambda) * q$$

$$H(\lambda) = \Phi(\lambda) * q * E(eV)$$

where Φ(λ), H(λ) are the photon flux and the power density of the indoor light sources.

Shunt resistance measurement: The shunt resistance of the corresponding devices were obtained from the dark *J-V* curves. These curves can be divided into three regions according to the change of the slope: parallel resistance region, injection region and series resistance region. The behavior of the curve in these regions is dominated by the shunt resistance, diode ideality, and series resistance, respectively. The differential resistance in the parallel resistance region is equal to the corresponding shunt resistance (Fig. S19)[4-6]

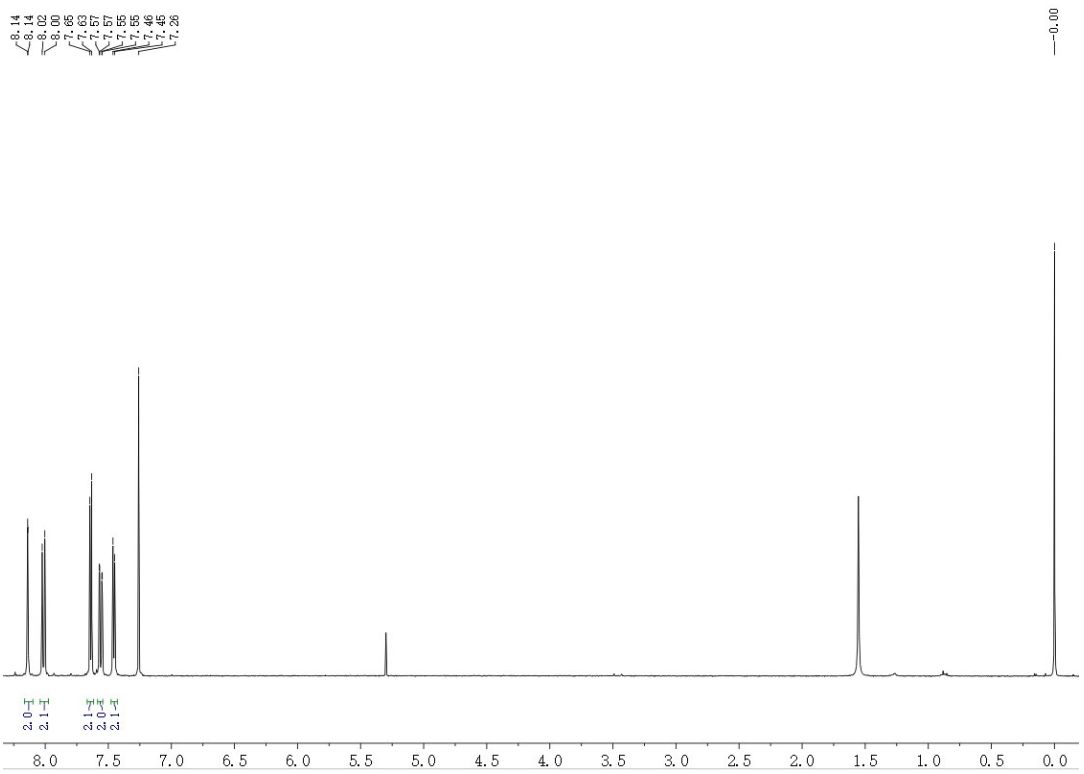

Fig. S1. ^{1}H NMR (400 MHz, $CDCl_3$) of compound 2

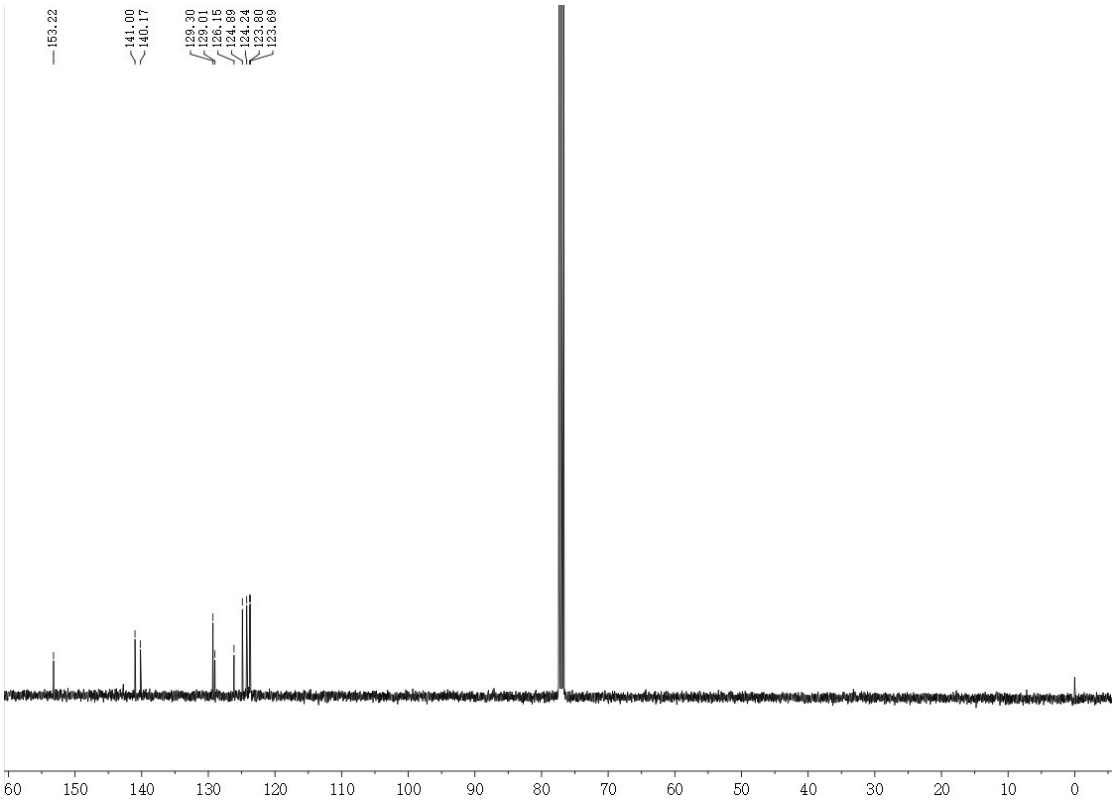

Fig. S2.^{13}C NMR (101 MHz, $CDCl_3$) of compound 2.

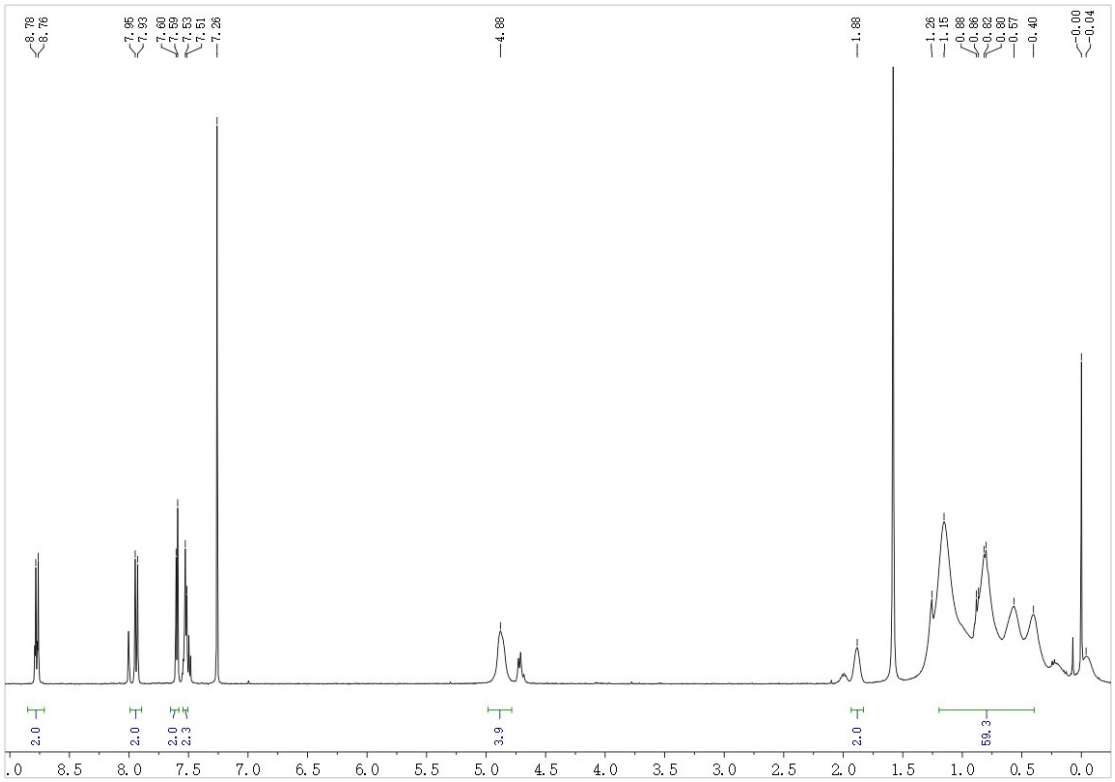

Fig. S3. ^{1}H NMR (400 MHz, $CDCl_3$) of compound 3.

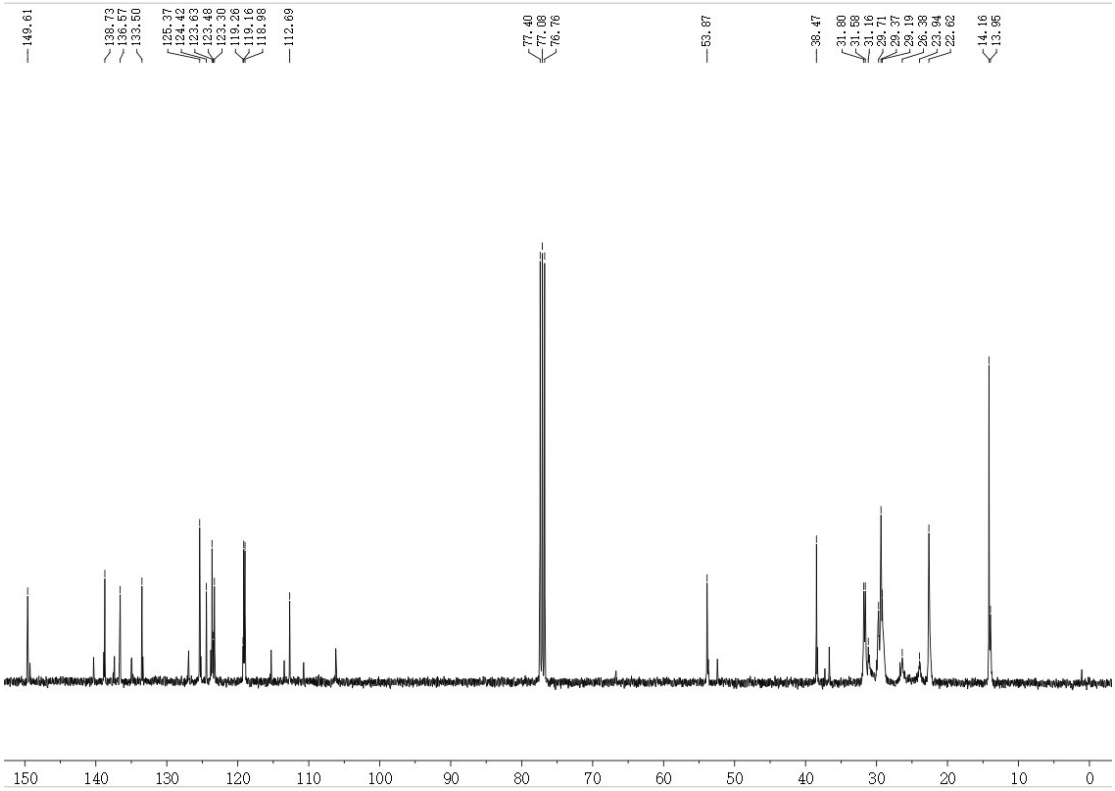

Fig. S4.^{13}C NMR (101 MHz, $CDCl_3$) of compound 3.

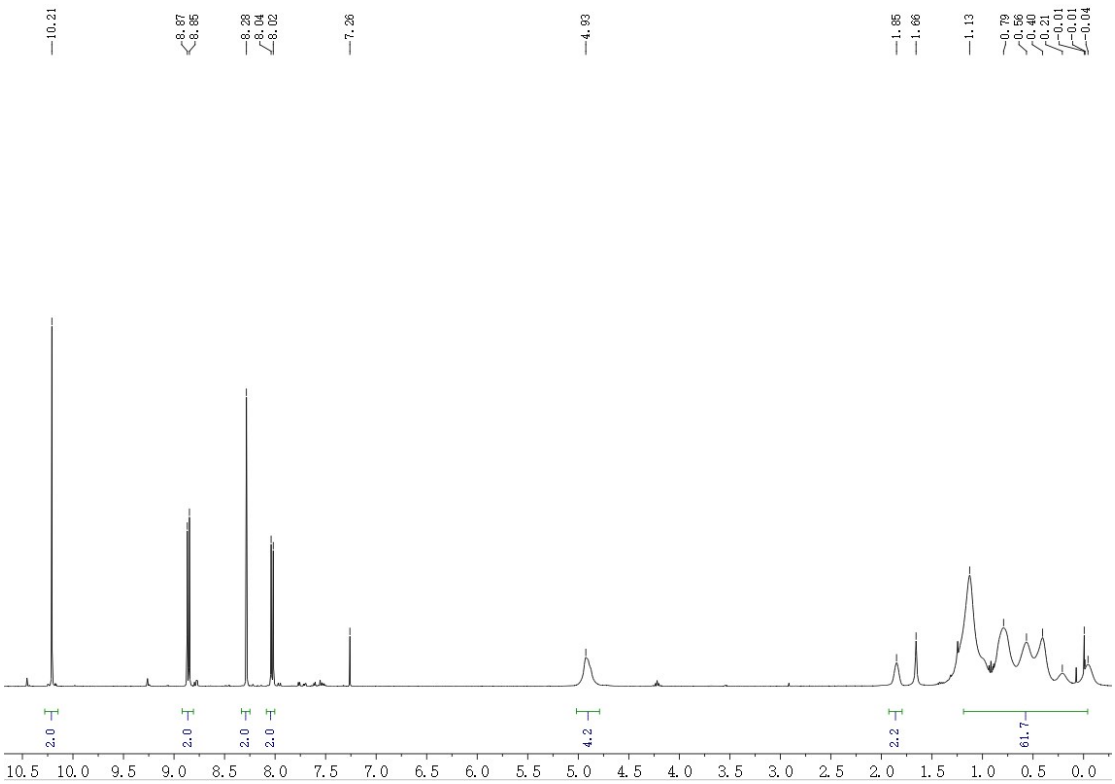

Fig. S5. ^{1}H NMR (400 MHz, $CDCl_3$) of compound 4.

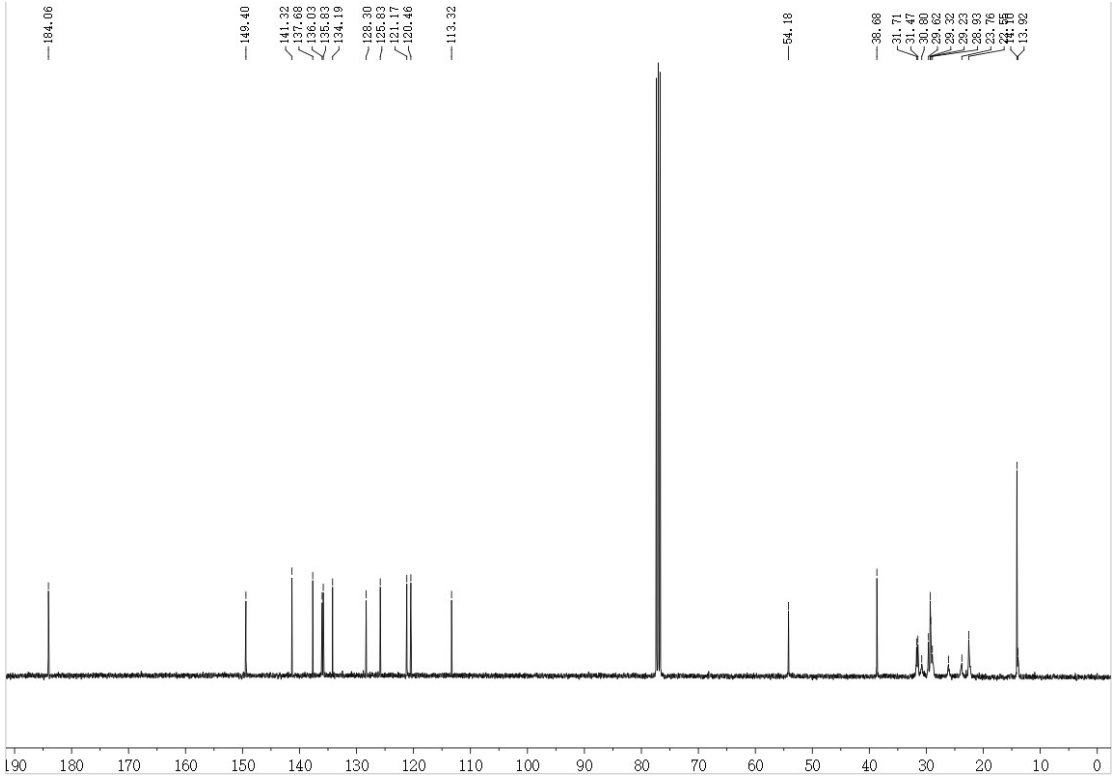

Fig. S6.^{13}C NMR (101 MHz, $CDCl_3$) of compound 4.

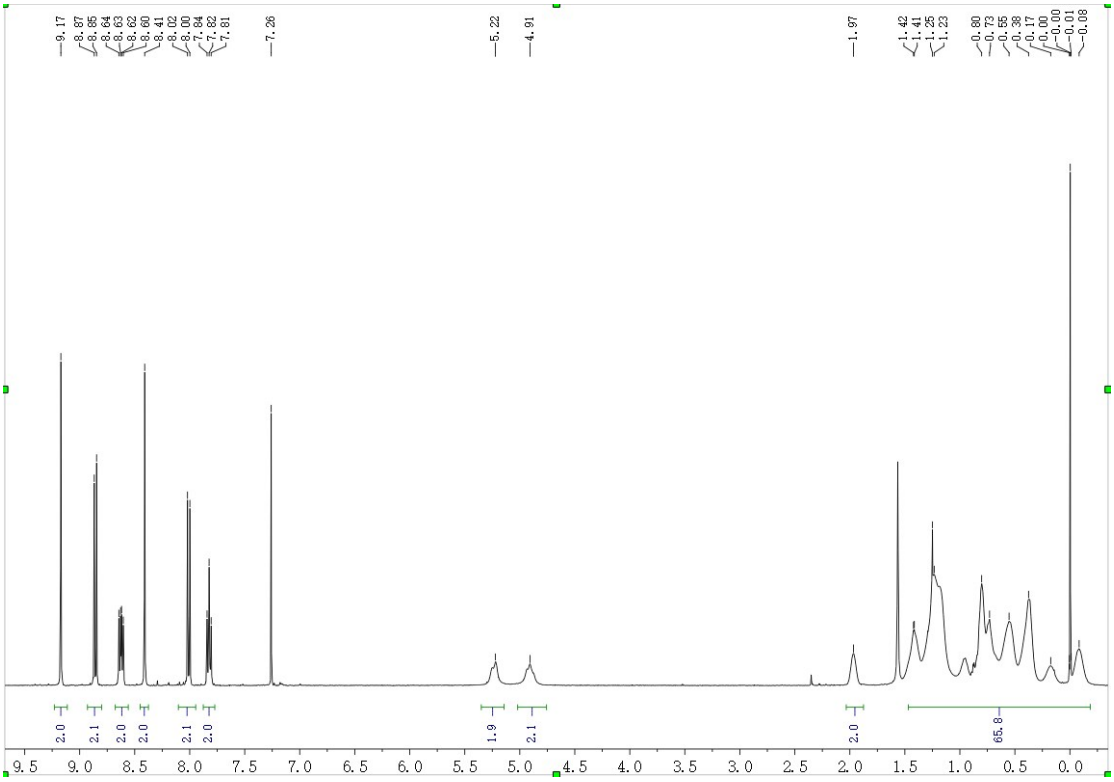

Fig. S7. ^{1}H NMR (400 MHz, $CDCl_3$) of compound LBT-DF.

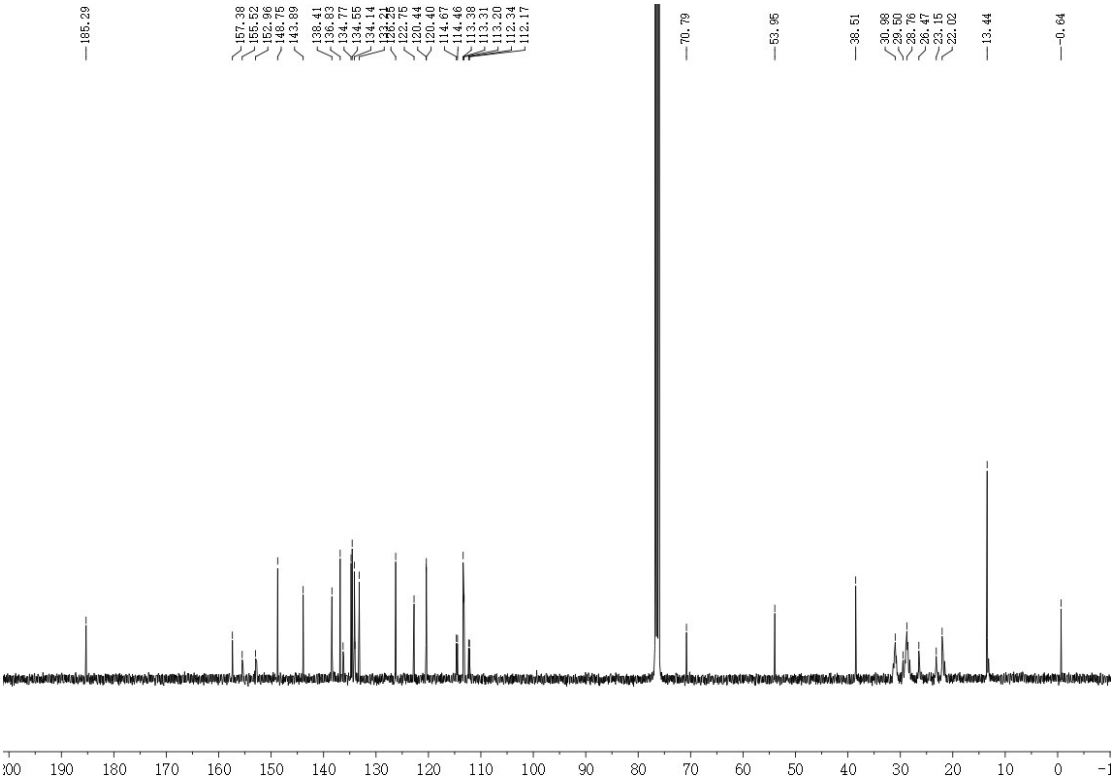

Fig. S8.^{13}C NMR (101 MHz, $CDCl_3$) of compound LBT-DF.

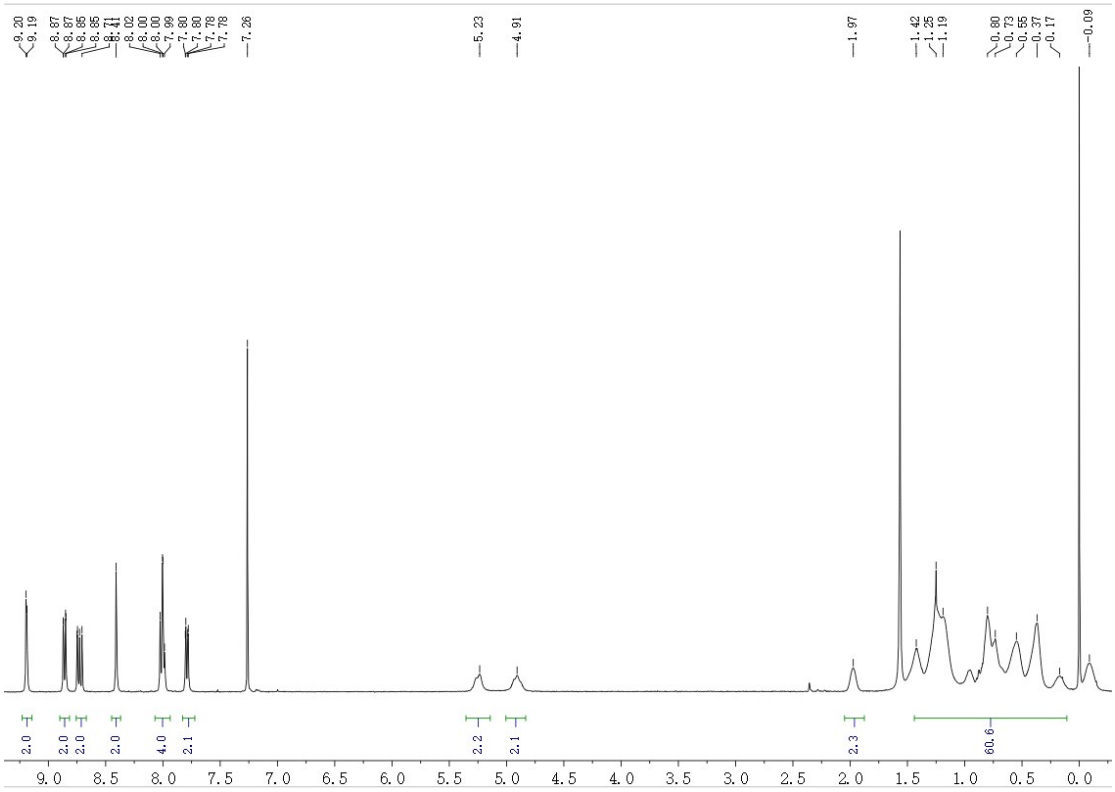

Fig. S9. ^{1}H NMR (400 MHz, $CDCl_3$) of compound LBT-SCl.

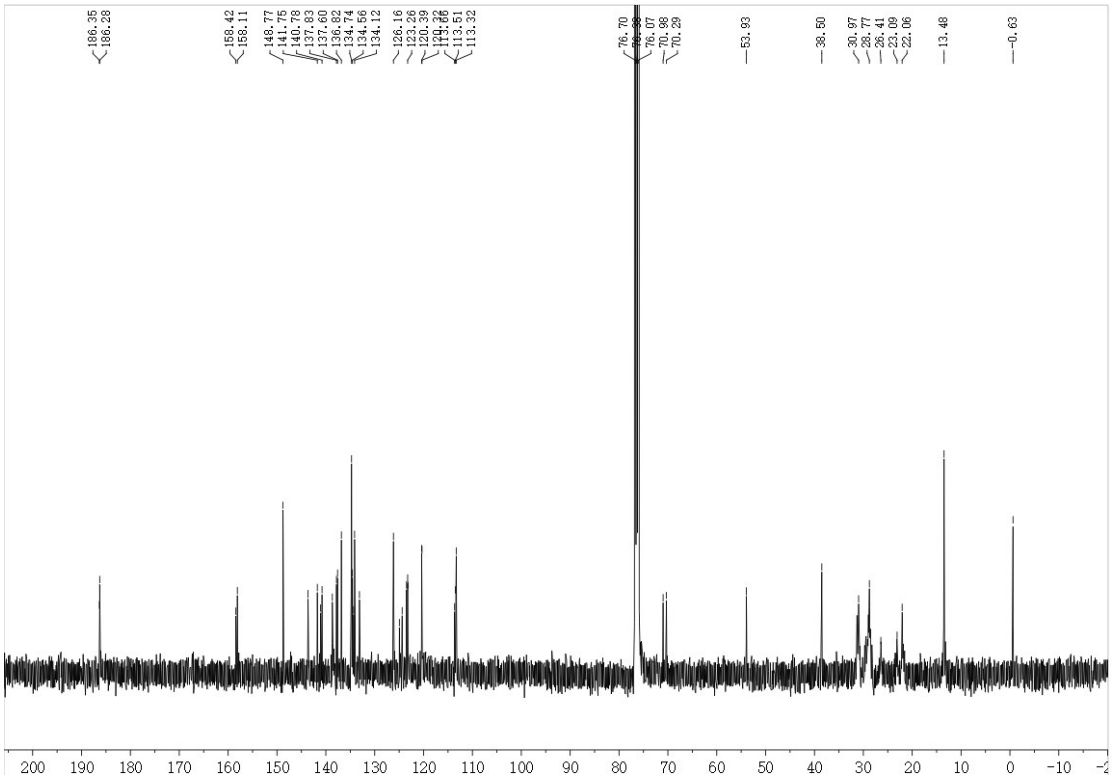

Fig. S10.^{13}C NMR (101 MHz, $CDCl_3$) of compound LBT-SCl.

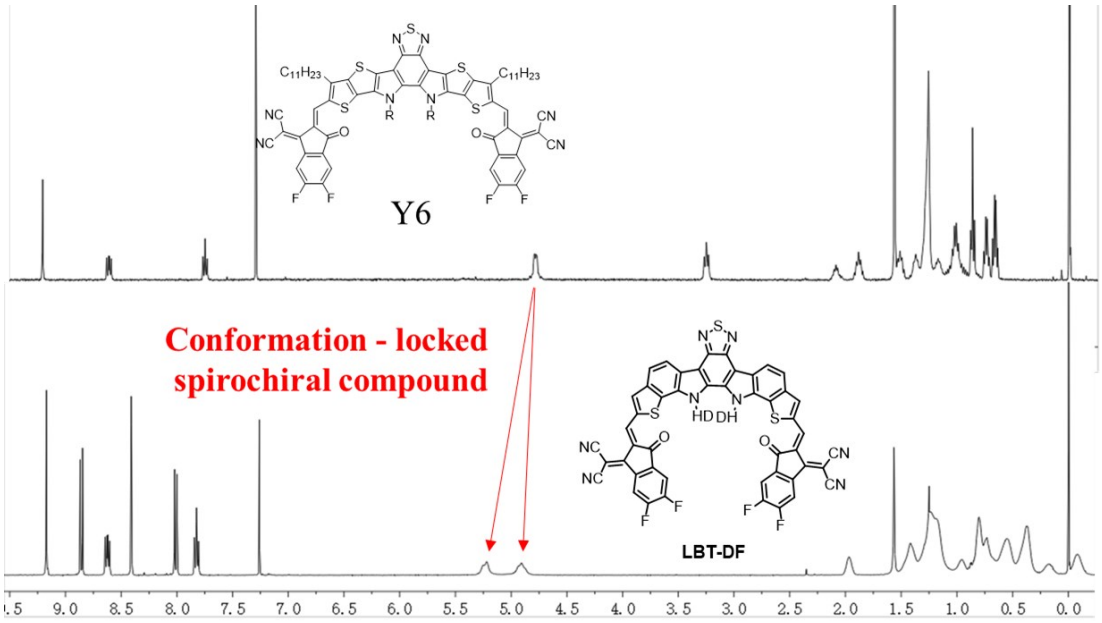

Fig. S11. The ^{1}H NMR of Y6 and LBT-DF.

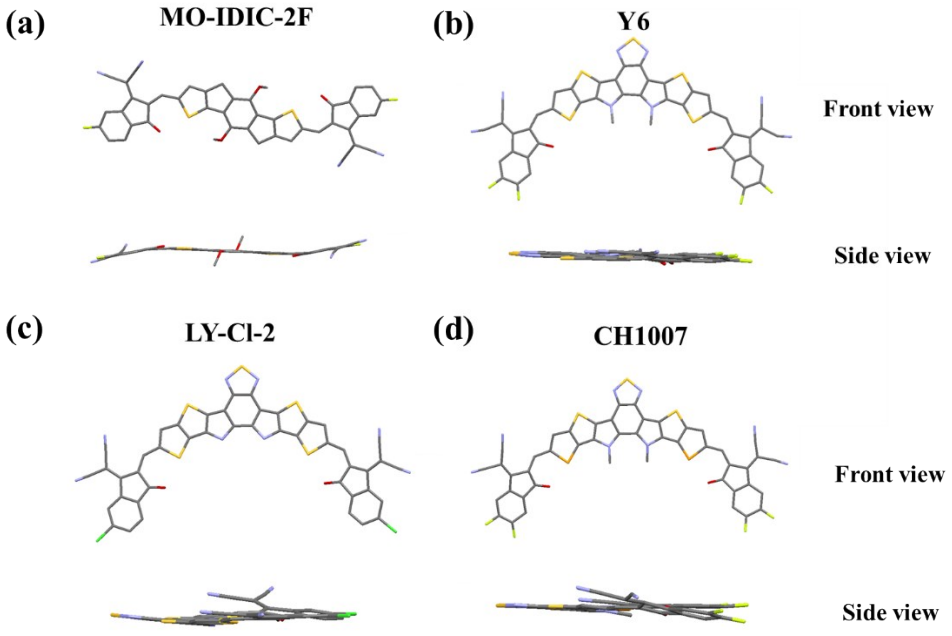

Fig. S12. Front and side view of (a) MO-IDIC-2F, (b) Y6, (c) LY-Cl-2, (d) CH1007.

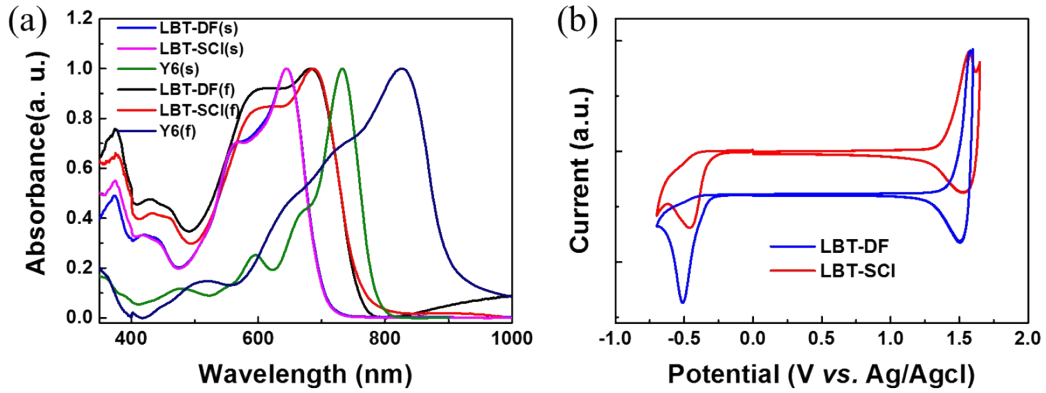

Fig. S13. (a) Absorption spectra of LBT-DF, LBT-SCl and Y6 in chloroform solutions and films state, (b) cyclic voltammograms of LBT-DF and LBT-SCl.

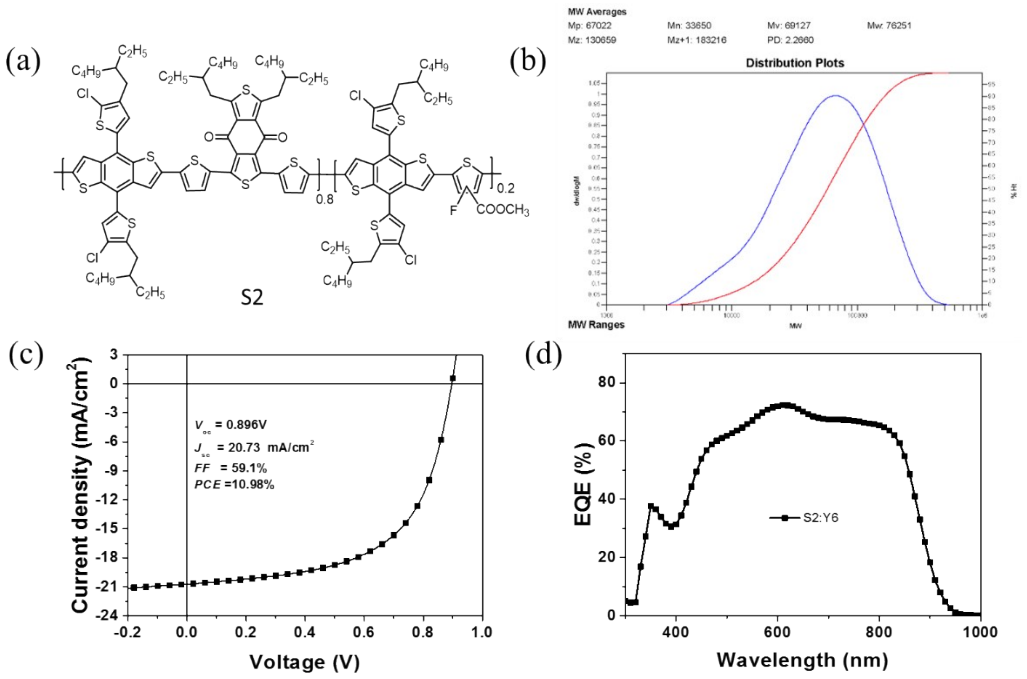

Fig. S14. (a)The structure of polymer donor S2, (b) the GPC data of S2, (c) the *J-V* curves of the OPVs based on S2:Y6 under the illumination of AM 1.5 G, 100 mW cm^{-2}, (d) the EQE spectra of the OPVs based on S2: Y6.

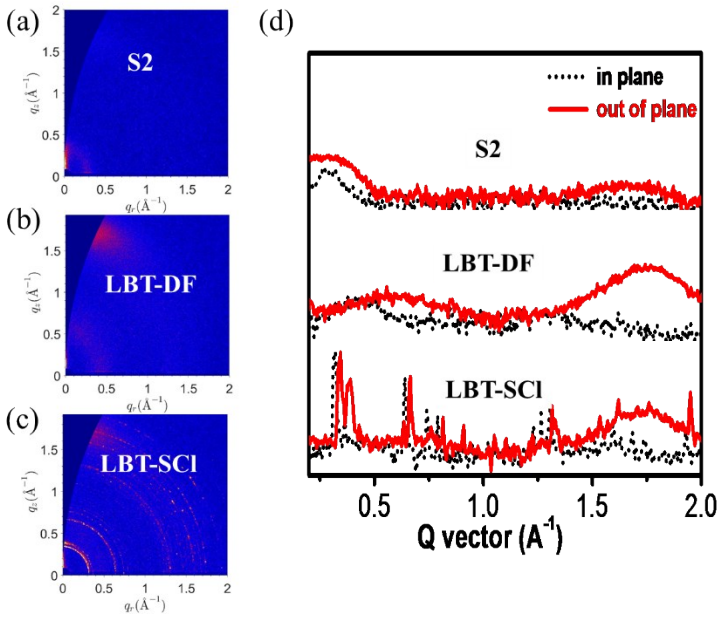

Fig. S15. 2D GIWAXS patterns of (a) S2 film (b) LBT-DF film and (c) LBT-SCl film, (d) Line cuts of the GIWAXS images of S2, LBT-DF, and LBT-SCl films.

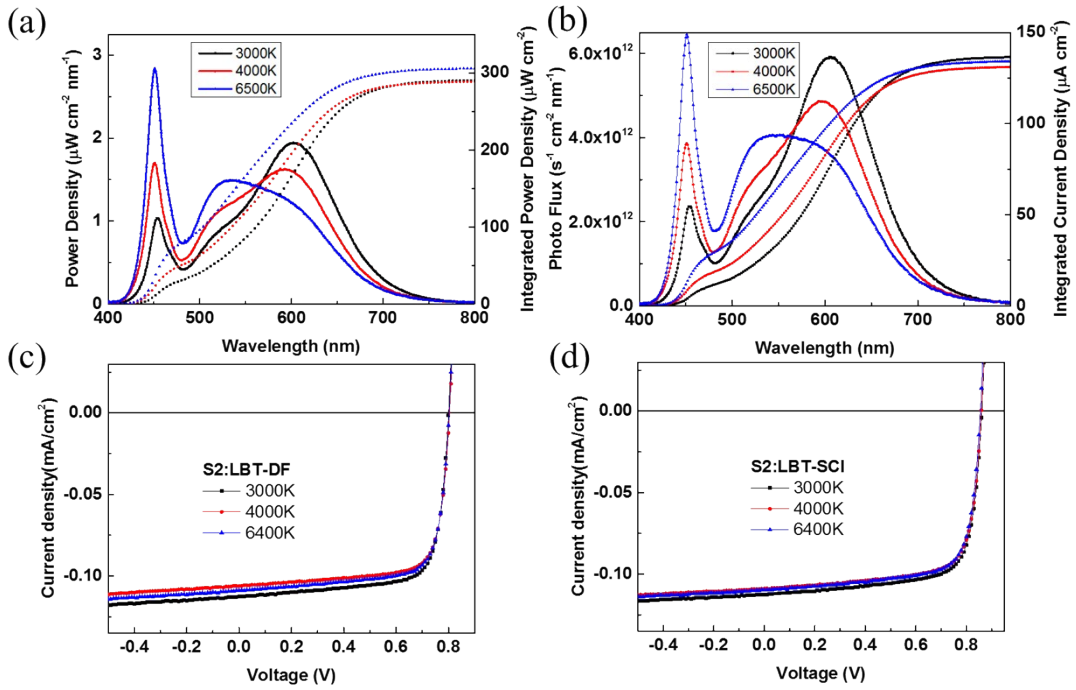

Fig. S16. (a) The emission power spectrum and integrated power density curve of white LEDs at 1000 lux, (b) the photon flux spectrum of white LEDs at 1000 lux and the integral current density. The *J-V* characteristic curves of (c) S2: LBT-DF and (d) S2: LBT-SCl under white LEDs at 1000 lux.

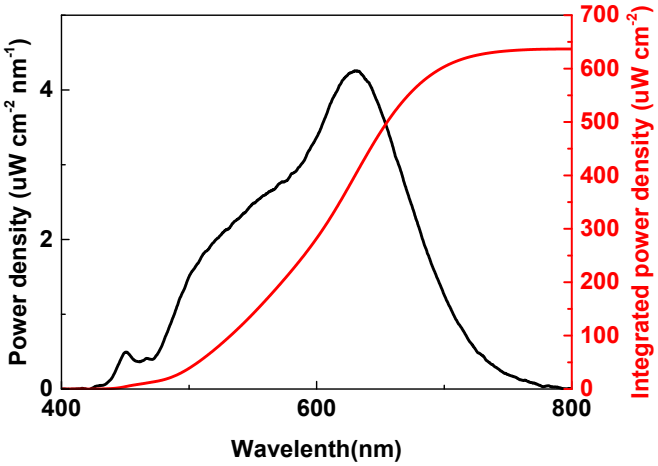

Fig. S17. The emission power spectrum and integrated power density curve of the 2600K LED at 2000lux.

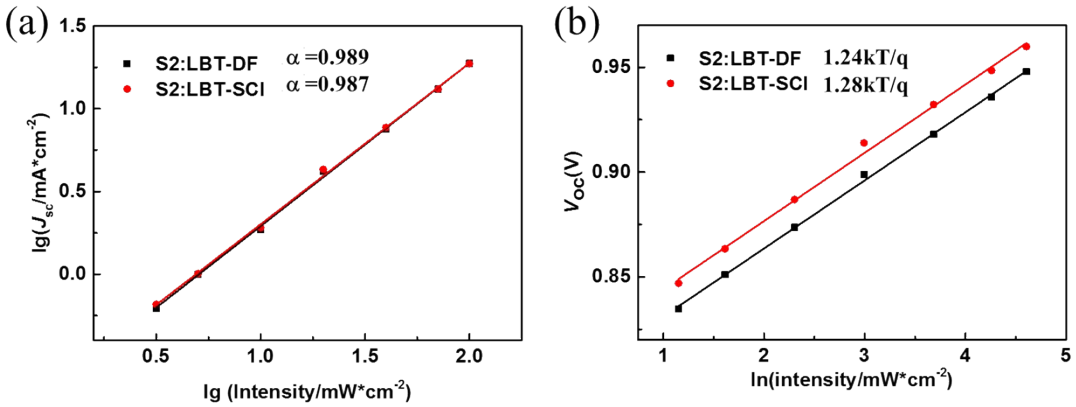

Fig. S18. (a) Light-intensity-dependent J_{sc} experiments on S2: LBT-DF and S2:LBT-SCl, (b) the light-intensity-dependent V_{oc} experiments on S2:LBT-DF and S2:LBT-SCl.

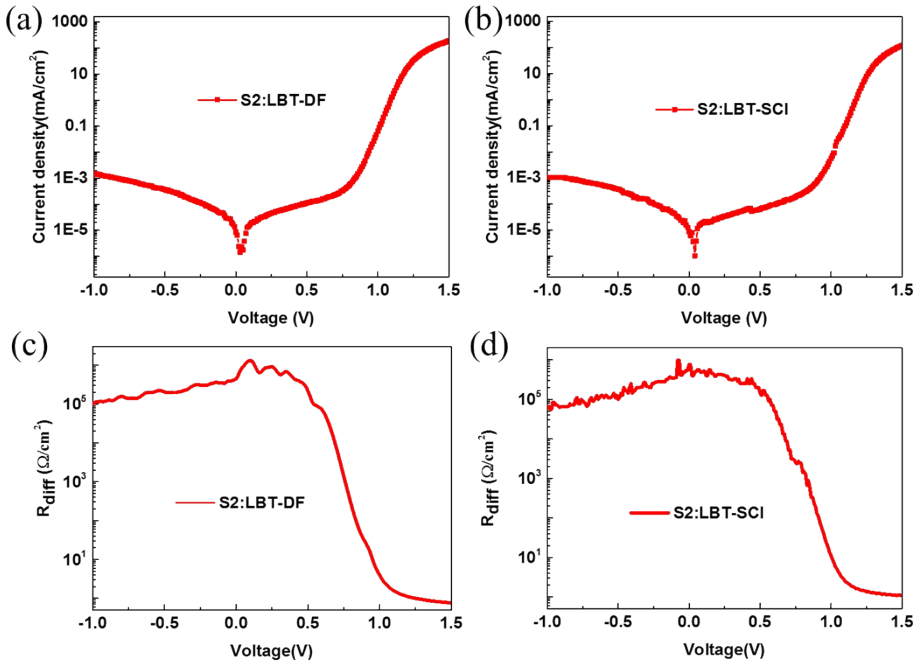

Fig. S19. The dark *J-V* curves of (a) S2: LBT-DF and (b) S2: LBT-SCl devices, the differential resistances derived from the dark *J-V* curves of (c) S2: LBT-DF and (d) S2: LBT-SCl devices.

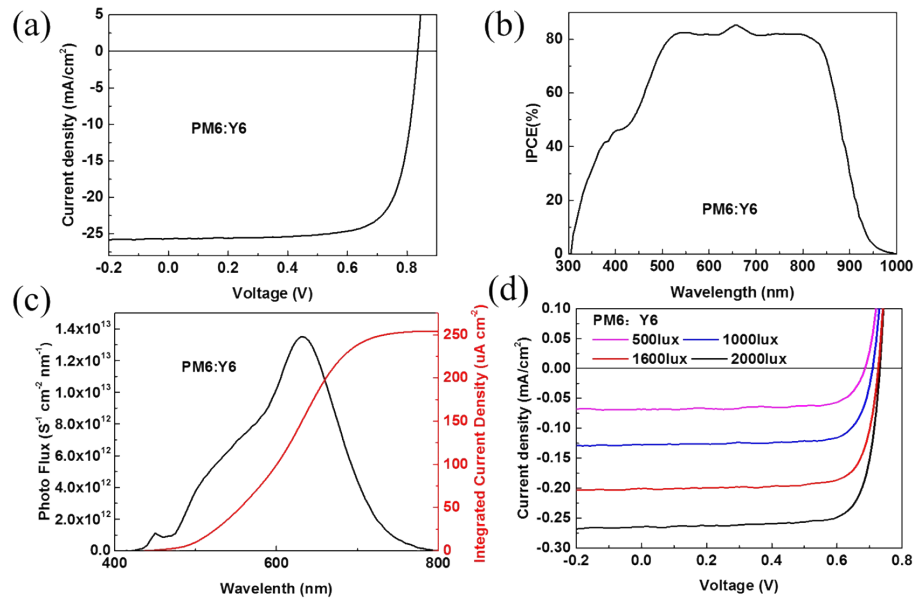

Fig. S20. (a) The *J-V* curves of PM6:Y6 under AM 1.5 G illumination, (b) the IPCE spectra of PM6:Y6, (c) the *J-V* characteristic curves of PM6:Y6 under different indoor light intensity, (d) photo flux spectrum of 2600K LED lamp at 2000lux and the integral current density of PM6:Y6 under that condition.

Table S1. Crystal data and structure refinement for LBT-DF.

Identification code	LBT-DF
Empirical formula	$C_{80}H_{74}F_4N_8O_2S_3$
Formula weight	1351.65
Temperature/K	173.0(1)
Crystal system	monoclinic
Space group	I2/a
a/Å	9.93013(9)
b/Å	33.0819(3)
c/Å	23.3061(3)
α/°	90
β/°	94.7559(10)
γ/°	90
Volume/Å^3	7629.88(13)
Z	4
ρ_{calc}g/cm^3	1.177
μ/mm^{-1}	1.370
F(000)	2840.0
Crystal size/mm^3	0.4 × 0.25 × 0.03
Radiation	Cu Kα (λ = 1.54184)
2Θ range for data collection/°	7.612 to 163.862
Index ranges	-12 ≤ h ≤ 12, -41 ≤ k ≤ 41, -28 ≤ l ≤ 26
Reflections collected	56007
Independent reflections	8033 [R_{int} = 0.0426, R_{sigma} = 0.0195]
Data/restraints/parameters	8033/128/514
Goodness-of-fit on F^2	1.032
Final R indexes [I>=2σ (I)]	R_1 = 0.0516, wR_2 = 0.1569
Final R indexes [all data]	R_1 = 0.0564, wR_2 = 0.1648
Largest diff. peak/hole / e Å^{-3}	0.62/-0.49

Table S2. Physicochemical properties of LBT-DF and LBT-SCl.

	λ_{max}[a] (nm)	λ_{edge}[a] (nm)	E_g^{opt}[b] (eV)	E_{HOMO}[c] (eV)	E_{LUMO}[c] (eV)
LBT-DF	681	758	1.64	-5.82	-4.01
LBT-SCl	688	766	1.62	-5.75	-3.96

[a]Absorption of the films. [b] Calculated from the absorption edge of the polymer films: $E_g^{opt} = 1240/\lambda_{edge}$. [c] Calculated according to the equation $E_{LUMO/HOMO} = -e(E_{red/ox} + 4.36)$ (eV)

Table S3. Charge carrier mobilities of the PSCs based on neat films of acceptors and blend films of S2: acceptors with thermal annealing at 100 °C for 5 min.

	μ_h (cm^2 V^{-1} s^{-1})	μ_e (cm^2 V^{-1} s^{-1})
S2:LBT-DF	9.53×10^{-4}	6.58×10^{-4}
S2:LBT-SCl	9.22×10^{-4}	5.26×10^{-4}
LBT-DF		4.86×10^{-4}
LBT-SCl		4.57×10^{-4}

Table S4. Device parameters of S2:LBT-DF under white LEDs with different colour temperature at 1000 lux.

Active layer	Color Temperature	P_{in} (mW cm^{-2})	V_{oc} (V)	J_{sc} (mA cm^{-2})	FF (%)	PCE (%)	J_{cal} [a] (mA cm^{-2})
S2:LBT-DF	3000K	0.290	0.800	0.113	75.1	23.3	0.109
	4000K	0.289	0.804	0.106	75.4	22.3	0.104
	6400K	0.306	0.802	0.109	74.8	21.3	0.104

[a] J_{cal} was obtained by integrating the IPCE spectrum over the light source.

Table S5. Device parameters of S2:LBT-SCl under white LEDs with different colour temperature at 1000 lux.

Active layer	Color Temperature	P_{in} (mW cm^{-2})	V_{oc} (V)	J_{sc} (mA cm^{-2})	FF (%)	PCE (%)	J_{cal} [a] (mA cm^{-2})
S2:LBT-SCl	3000K	0.290	0.861	0.112	73.9	24.7	0.109
	4000K	0.289	0.859	0.209	73.9	24.0	0.103
	6400K	0.306	0.855	0.110	73.7	22.6	0.104

[a] J_{cal} was obtained by integrating the IPCE spectrum over the light source.

Table S6. Device parameters of PM6: Y6 under AM 1.5G condition and different light intensity under a 2600K LED lamp

Active layer		P_{in} (mW cm^{-2})	V_{oc} (V)	J_{sc} (mA cm^{-2})	FF (%)	PCE (%)	J_{cal} [a] (mA cm^{-2})
PM6:Y6	One sun	—	0.836	25.66	75.1	16.1	25.19
	500lux	0.159	0.684	0.0636	76.2	20.9	0.0634
	1000lux	0.318	0.708	0.1270	78.6	22.2	0.1269
	1600lux	0.509	0.725	0.2049	79.1	23.1	0.2032
	2000lux	0.637	0.731	0.2624	79.0	23.8	0.2539

[a] J_{cal} was obtained by integrating the IPCE spectrum over the light source.

1. O. Dolomanov, L.J. Bourhis, R.J. Gildea, J. Howard and H. Puschmann, *J. Appl. Cryst.,* 2009, **42**, 339-341.
2. L. Bourhis, O. Dolomanov, R. Gildea, J. Howard and H. Puschmann, *Acta Cryst.* 2015, A71, 59-75.
3. G.M. Sheldrick, *Acta Cryst.* 2015, C71, 3-8.
4. Y. Chang, T.-K. Lau, P.C.Y. Chow, N. Wu, D. Su, W. Zhang, H. Meng, C. Ma, T. Liu, K. Li, X. Zou, K. S. Wong, X. Lu, H. Yan and C. Zhan *J. Mater. Chem. A.,* 2020, **8**, 3676-3685.
5. C. M. Proctor and T. Nguyen, *Appl. Phys. Lett.*, 2015, **106**, 083301.
6. J. Vollbrecht, V.V. Brus, S. Ko, J. Lee, A. Karki, D. X. Cao, K. Cho, G. C. Bazan, and T. Nguyen, *Adv. Energy Mater.* 2019, **9,** 1901438